0.1 Kinetic gas theory

The kinetic theory of gases was initiated with the development of the Maxwell-Boltzmann equations in the mid- to late 19th century.[1] The equations are based in statistical mechanics, and consider the effects of collisions between particles. The solutions to these equations, developed by Chapman and Enskog in the early 20th century, are termed the Chapman-Enskog or Enskog solutions, and the resulting theory is referred to as Enskog theory. This theory has later been expanded and elaborated upon by Chapman and Cowling, among many others.[2,3]

The theory is highly mathematical in nature and at times difficult to follow. Nevertheless the goal of this section is to present a pedagogical summary of the derivations and results integral to this report. For a complete, rigorous explanation of the theory, the reader is referred to the text by Chapman and Cowling.[1] It is worth mentioning that despite being a compressed summary, this section is characterised by a large volume of notation and definitions. This is due to the theory itself being characterised by multiply nested definitions, and notation that requires explaining. Note also that the notation employed here differs somewhat from that of Chapman and Cowling so as to remain consistent throughout the report.

The goal of this section is to arrive at a set of explicit equations that can be solved for the interdiffusion- and thermal diffusion coefficients, such that a value for α_T^{ig} may be supplied to the Kempers-model. This will require a rigorous definition of how these coefficients relate to the average velocities of particles in a mixture. It may be fruitful to have the final result in mind when reading, to have this as a reference point as new variables and functions are introduced. By the end of this section the integrals

$$\begin{aligned} D_{12} \equiv & \frac{\rho_1\rho_2}{3\rho}\{\mathbf{D},\mathbf{D}\} \\ = & \frac{\rho_1\rho_2}{3\rho^3}\int \mathbf{D}_1 \iiint f_1^{(0)} f_{1'}^{(0)} (\mathbf{D}_1 + \mathbf{D}_{1'} - \mathbf{D}_1' - \mathbf{D}_{1'}') b\mathrm{d}b\mathrm{d}\epsilon\mathrm{d}\mathbf{u}_{1'}\mathrm{d}\mathbf{u}_1 \\ & + \frac{\rho_1\rho_2}{6\rho^3}\iiiint f_1^{(0)} f_2^{(0)} (\mathbf{D}_1 + \mathbf{D}_2 - \mathbf{D}_1' - \mathbf{D}_2')^2 b\mathrm{d}b\mathrm{d}\epsilon\mathrm{d}\mathbf{u}_1\mathrm{d}\mathbf{u}_2 \\ & + \frac{\rho_1\rho_2}{3\rho^3}\int \mathbf{D}_2 \iiint f_2^{(0)} f_{2'}^{(0)} (\mathbf{D}_2 + \mathbf{D}_{2'} - \mathbf{D}_2' - \mathbf{D}_{2'}') b\mathrm{d}b\mathrm{d}\epsilon\mathrm{d}\mathbf{u}_{2'}\mathrm{d}\mathbf{u}_2 \end{aligned} \tag{0.1}$$

$$\begin{aligned} D_T \equiv & \frac{\rho_1\rho_2}{3\rho}\{\mathbf{D},\mathbf{A}\} \\ = & \frac{\rho_1\rho_2}{3\rho^3}\int \mathbf{A}_1 \iiint f_1^{(0)} f_{1'}^{(0)} (\mathbf{D}_1 + \mathbf{D}_{1'} - \mathbf{D}_1' - \mathbf{D}_{1'}') b\mathrm{d}b\mathrm{d}\epsilon\mathrm{d}\mathbf{u}_{1'}\mathrm{d}\mathbf{u}_1 \\ & + \frac{\rho_1\rho_2}{6\rho^3}\iiiint f_1^{(0)} f_2^{(0)} (\mathbf{D}_1 + \mathbf{D}_2 - \mathbf{D}_1' - \mathbf{D}_2')(\mathbf{A}_1 + \mathbf{A}_2 - \mathbf{A}_1' - \mathbf{A}_2') b\mathrm{d}b\mathrm{d}\epsilon\mathrm{d}\mathbf{u}_1\mathrm{d}\mathbf{u}_2 \\ & + \frac{\rho_1\rho_2}{3\rho^3}\int \mathbf{A}_2 \iiint f_2^{(0)} f_{2'}^{(0)} (\mathbf{D}_2 + \mathbf{D}_{2'} - \mathbf{D}_2' - \mathbf{D}_{2'}') b\mathrm{d}b\mathrm{d}\epsilon\mathrm{d}\mathbf{u}_{2'}\mathrm{d}\mathbf{u}_2 \end{aligned} \tag{0.2}$$

will be defined, and a method for approximating their value will be introduced.

0.1.1 The Boltzmann-equations

To begin, the Maxwell-Boltzmann equations are derived by assuming that collisions - i.e. interactions between particles, occupy only a very small amount of a particles life time. This gives rise to a differential equation for the velocity distribution function $f_i = f_i(\mathbf{u}_i, \mathbf{r}, t)$, describing the probability of finding a particle of species i with velocity $\mathbf{u}_i$ at position $\mathbf{r}$ at time t. This equation reads

$$\frac{\partial f_i}{\partial t} + \mathbf{u}_i \nabla f_i + \mathbf{F_i}\frac{\partial f_i}{\partial \mathbf{u}_i} = \frac{\partial_e f_i}{\partial t} \tag{0.3}$$

where $\mathbf{F}$ denotes an external force on the particle and $\frac{\partial_e f}{\partial t}$ describes the rate of change owing to encounters between molecules. The latter of these may be expanded as a sum over the change due to encounters of

different types, that is

$$\frac{\partial_e f_i}{\partial t} = \sum_j \left(\frac{\partial_e f_i}{\partial t} \right)_j \tag{0.4}$$

where subscript j denotes the particle type that particle i encounters, and the sum runs over all particle species. To describe this differential, a description of the dynamics of a binary encounter between particles is required. This description is done through a set of rather involved geometric considerations that are difficult to summarise shortly. Therefore, only a summary of the variables involved, their significance and their dependencies are included here, shown graphically in Figure 0.1. Let $\mathbf{g}_{12}$ and $\mathbf{g}_{21}$ denote the initial velocity

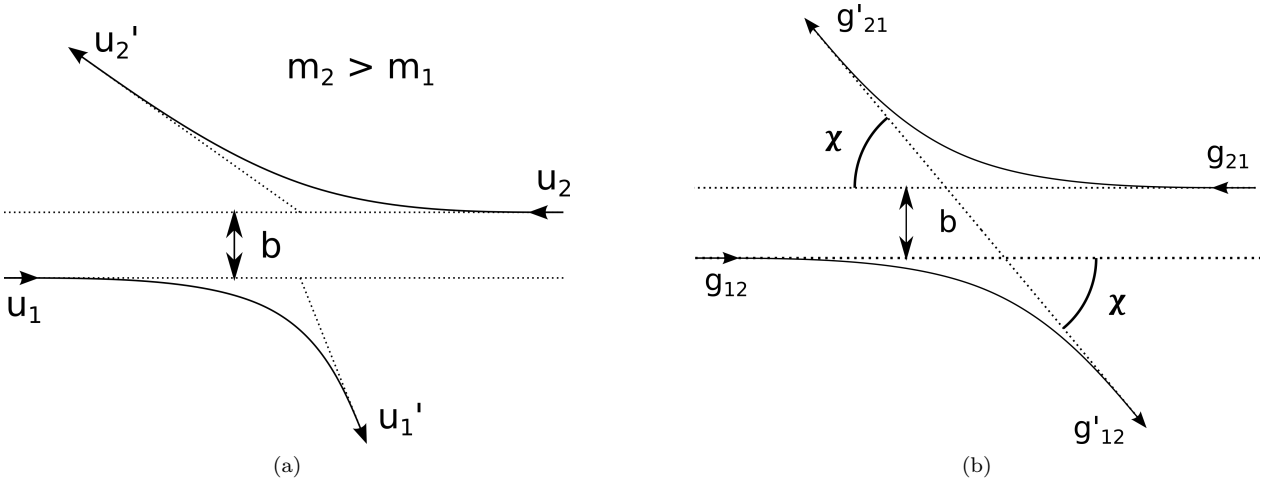

Figure 0.1: The geometry of a binary encounter.

of particle 1 relative to 2, and 2 relative to 1. Evidently $\mathbf{g}_{12} = \mathbf{u}_1 - \mathbf{u}_2 = -\mathbf{g}_{12}$. Primes on the velocities will denote the post-collision velocities, $\mathbf{g}'_{12} = \mathbf{u}'_1 - \mathbf{u}'_2 = -\mathbf{g}'_{12}$. Due to conservation of energy and momentum, the encounter can be completely described by the change in direction of the relative velocities, as the centre of mass velocity is constant. Further, assume that the forces acting between the particles act along the line connecting their centres of mass. For spherical particles this is clearly correct, but for chain-like molecules it cannot be expected to hold.

Now, let χ denote the deflection angle of the relative velocity, that is $\cos\chi = \mathbf{g}_{12} \cdot \mathbf{g}'_{12}$. To describe χ, one must also define the impact parameter b. This can be thought of as the "closest passing distance" the particles would have had if they had been non-interacting point particles, as visualised in Figure 0.1. It is clear that χ is a function of b, and that the functional form is dependent on the intermolecular potential. For a hard-sphere potential, an analytical expression can be derived without extended effort. For other potentials however, the dependency on $\mathbf{g}_{12}$ and the molecular masses requires one to employ numerical methods. For now, χ will be left as some function of $\mathbf{g}_{12}$, b, m_1 and m_2.

Finally, to expand the geometry of Figure 0.1 to three dimensions, define a cylindrical coordinate system centred on particle 1, with the vertical axis perpendicular to $\mathbf{g}_{12}$, such that b takes the role of the radial coordinate. Denote the angular coordinate of this system as ϵ. This coordinate system is shown in Figure 0.2. Following these geometric considerations it can be shown that

$$\left(\frac{\partial_e f_i}{\partial t} \right)_j = \iiint \left(f'_i f'_j - f_i f_j \right) b \mathrm{d}b \mathrm{d}\epsilon \mathrm{d}\mathbf{u}_j. \tag{0.5}$$

The truncation of an interaction potential at some distance now amounts to limiting the integral over $\mathrm{d}b$ to that distance. The case of $i = j$ follows the exact same row of arguments as the case $i \neq j$, but the notation

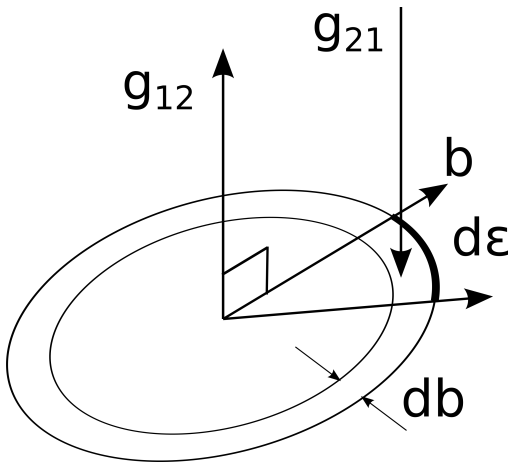

Figure 0.2: Cylindrical coordinate system to describe an encounter.

employed can quickly lead to confusion. The integral in Equation (0.5) passes over $\mathbf{u}_j$, and is therefore a function only of $\mathbf{u}_i$. If $i = j$, recognise that the integral still only passes over the velocity of one particle in the colliding pair, such that it is still a function of the velocity of the other particle. Notation-wise Chapman and Cowling solve this by denoting the velocity of the two particles as $\mathbf{u}$ and $\mathbf{u}_i$ and writing

$$\left(\frac{\partial_e f_i}{\partial t}\right)_i = \iiint \left(f_i' f' - f_i f\right) b\mathrm{d}b\mathrm{d}\epsilon\mathrm{d}\mathbf{u}. \tag{0.6}$$

To avoid confusion as to what function f at any time refers to, the notation employed here will denote the velocity of the two particles as $\mathbf{u}_{i'}$ and $\mathbf{u}_i$, such that

$$\left(\frac{\partial_e f_i}{\partial t}\right)_i = \iiint \left(f_i' f_{i'}' - f_i f_{i'}\right) b\mathrm{d}b\mathrm{d}\epsilon\mathrm{d}\mathbf{u}_{i'}. \tag{0.7}$$

For brevity, the integral in equation (0.5) will later be written as

$$-\left(\frac{\partial_e f_i}{\partial t}\right)_j \equiv \begin{cases} J_{ij}(f_i f_j) & i \neq j \\ J_i(f_{i'} f_i) & i = j \end{cases} \tag{0.8}$$

Where the prime in $J_i(f_{i'} f_i)$ indicates the variable of integration, the differentiation will become important later. The left hand side of equation (0.3) will be written as $\mathscr{D}_i f_i$, thus the Boltzmann equation for a single-component (simple) gas reads

$$\mathscr{D}_i f_i + J_i(f_{i'} f_i) = 0 \tag{0.9}$$

0.1.2 The first approximation for a simple gas

Now that the notation and formulation of the Boltzmann-equations has been established, the time is ripe for introducing the Enskog solution method. Assume that the true solution, f, of equation (0.3) can be written as an infinite series $f = \sum_{r=0}^{\infty} f^{(r)}$. The operators $\mathscr{D}$ and J can also be subdivided. First, introduce the operator $\frac{\partial_r}{\partial t}$, with the property

$$\frac{\partial \varphi}{\partial t} \equiv \sum_r \frac{\partial_r \varphi}{\partial t}, \qquad \varphi = \{\rho, T, \mathbf{u}^n\} \tag{0.10}$$

where $\mathbf{u}^n$ denotes the mole average velocity of the gas, and ρ denotes the number density of the gas. For the formal definition of $\frac{\partial_r}{\partial t}$ the reader is referred to Chapman and Cowling, pp. 116.[1] Enskog now subdivides

the operator $\mathscr{D}$ such that

$$\begin{aligned}\mathscr{D}_1 f_1 &= \sum_r \mathscr{D}^{(r)}, \qquad \mathscr{D}^{(0)} = 0 \\ \mathscr{D}_1^{(r)} &= \sum_{i=0}^{r-1} \frac{\partial_r f_1^{(r-1-i)}}{\partial t} + \mathbf{u}\cdot\nabla f_1^{(r-1)} + \mathbf{F}_1\cdot\nabla f_1^{(r-1)}, \qquad r>0.\end{aligned} \tag{0.11}$$

Similarly, J can be subdivided such that

$$J_1^{(r)} = \sum_{i=0}^{r} J_1(f_{1'}^{(i)} f_1^{(r-i)}). \tag{0.12}$$

It is important to note that this manner of subdividing $\mathscr{D}$ and J is a matter of choice, and that the key to the Enskog solution lies in choosing to subdivide them in this way. The result of the subdivision is that Equation (0.9) may be written as

$$\sum_r \mathscr{D}_1^{(r)} + J_1^{(r)} = 0 \tag{0.13}$$

This equation is fulfilled if $\mathscr{D}_1^{(r)} + J_1^{(r)} = 0, \forall\, r$, and the manner in which $\mathscr{D}$ and J have been subdivided ensures that each of these equations is solvable. The equation corresponding to $r=0$ becomes $J_1(f_{1'}^{(0)} f_1^{(0)}) = 0$, of which

$$f_1^{(0)} = \exp\left(\alpha^{(1)} + \boldsymbol{\alpha}^{(\mathbf{2})} m\mathbf{u}_1 + \alpha^{(3)}\frac{1}{2}mu_1^2\right) \tag{0.14}$$

is the general solution, with $\alpha^{(1)}, \boldsymbol{\alpha}^{(\mathbf{2})}$ and $\alpha^{(3)}$ arbitrary quantities independent of $\mathbf{u}_1$, and $u_1 = |\mathbf{u}_1|$ is the particle speed. Making some convenient choices for these, yields

$$f_1^{(0)} = \rho\left(\frac{m_1}{2\pi k_B T}\right)^{\frac{3}{2}} \exp\left(-\frac{m_1 U_1^2}{2k_B T}\right), \tag{0.15}$$

where $\mathbf{U}_i = \mathbf{u}_i - \mathbf{u}^n$ is the peculiar velocity of species i, and U is its magnitude, the peculiar speed. Note that $J_1(f^{(0)} f_1^{(0)}) = 0$ is the exact equation describing a gas in which collisions have no net effect on the velocity distribution function, such that $f^{(0)}$ is the velocity distribution function in a homogeneous (uniform) steady state gas. It is evident then, that to describe a non-uniform state, a solution for the second approximation $f^{(1)}$ must be found. Before moving on, note some properties of the velocity distribution function regarding the *summational invariants*, ρ, $m\mathbf{U}$ and $\frac{1}{2}mU^2$. That is, the number density, momentum and kinetic energy of the gas. These must all be conserved over time. It then follows that

$$\begin{aligned}\int f_1^{(0)} \mathrm{d}\mathbf{u}_1 = \rho_1 = \int f_1 \mathrm{d}\mathbf{u}_1 \\ \int (f_1 - f_1^{(0)}) \mathrm{d}\mathbf{u}_1 = 0\end{aligned} \tag{0.16}$$

and similarly for the other invariants,

$$\int (f_1 - f_1^{(0)})\varphi \mathrm{d}\mathbf{u}_1 = 0, \qquad \varphi = \{m\mathbf{U}_1, \frac{1}{2}mU_1^2\}. \tag{0.17}$$

Inserting for $f_1 = \sum_{r=0}^{\infty} f_1^{(r)}$ then yields

$$\sum_{r=1}^{\infty} \int f_1^{(r)} \varphi \mathrm{d}\mathbf{u}_1 = 0, \qquad \varphi = \{1, m\mathbf{U}_1, \frac{1}{2}mU_1^2\}. \tag{0.18}$$

This equation is clearly fulfilled if

$$\int f_1^{(r)} \varphi \mathrm{d}\mathbf{u}_1 = 0 \quad \forall \quad i>0, \qquad \varphi = \{1, m\mathbf{U}_1, \frac{1}{2}mU_1^2\}. \tag{0.19}$$

0.1.3 The second approximation for a simple gas

It can be shown that a valid second approximation to f can be written on the form $f_1^{(1)} = f_1^{(0)}\Phi_1^{(1)}$. Just like the first approximation, the second approximation satisfies Equation (0.13) if

$$\mathscr{D}_1^{(1)} + J_1^{(1)} = 0. \tag{0.20}$$

Here, $\mathscr{D}^{(1)}$ may be expanded as

$$\begin{aligned}\mathscr{D}_1^{(1)} &= f_1^{(0)}\left[\left(\frac{mU_1^2}{2k_BT} - \frac{5}{2}\right)\mathbf{U}_1\nabla\ln T + \frac{m}{k_BT}\mathbf{U}_1\overset{\circ}{\mathbf{U}}_1 : \nabla\mathbf{u}^n\right] \\ &= f_1^{(0)}\left[\left(\boldsymbol{\mathscr{U}}_1 - \frac{5}{2}\right)\mathbf{U}_1\nabla\ln T + \frac{m}{k_BT}\boldsymbol{\mathscr{U}}_1\overset{\circ}{\boldsymbol{\mathscr{U}}}_1 : \nabla\mathbf{u}^n\right]\end{aligned} \tag{0.21}$$

where for a 3d vector $\mathbf{v}$, $\overset{\circ}{\mathbf{vv}}$ is the operation

$$\overset{\circ}{\mathbf{vv}} = \begin{bmatrix} v_1 & & \\ & v_2 & \\ & & v_3\end{bmatrix}\begin{bmatrix} v_1 & v_2 & v3 \\ v_1 & v_2 & v3 \\ v_1 & v_2 & v3\end{bmatrix} - \frac{1}{3}v^2\underline{\boldsymbol{I}} \tag{0.22}$$

and for two matrices $\underline{\boldsymbol{\phi}}_1 : \underline{\boldsymbol{\phi}}_2 = \phi_{1,ij}\phi_{2,ji} = \sum_i\sum_j a_{ij}b_{ji}$ denotes the double dot product. $\boldsymbol{\mathscr{U}}_i$ is the dimensionless peculiar velocity $\boldsymbol{\mathscr{U}}_i \equiv \left(\frac{m_i}{2k_BT}\right)^{\frac{1}{2}}\mathbf{U}_i$. Further, the term $J^{(1)}$ can be expanded and rewritten as

$$\begin{aligned}J_1^{(1)} &= J_1(f_{1'}^{(0)}f_1^{(1)}) + J_1(f_{1'}^{(1)}f_1^{(0)}) \\ &= \rho^2 I_1\left(\Phi_1^{(1)}\right)\end{aligned} \tag{0.23}$$

where the integral $I_1\left(\Phi_1^{(1)}\right)$ has been introduced.

This is a convenient time to step aside and introduce some integral notation that will be heavily employed later. Recognise how Equations (0.1) and (0.2) are written with exactly this integral notation. Let F and G be functions defined on $\mathbf{u}_1$ and K be a function defined on $\mathbf{u}_1$ and $\mathbf{u}_2$. Then, using the notation $F_i = F(\mathbf{u}_i)$ and $K_{ij} = K_{ji} = K(\mathbf{u}_i, \mathbf{u}_j)$,

$$\begin{aligned}\rho_1^2 I_1(F) &\equiv \iiint f_1^{(0)}f_{1'}^{(0)}\left(F_1 + F_{1'} - F_1' - F_{1'}'\right)gb\mathrm{d}b\mathrm{d}\epsilon\mathrm{d}\mathbf{u}_{1'} \\ \rho_2^2 I_2(F) &\equiv \iiint f_2^{(0)}f_{2'}^{(0)}\left(F_2 + F_{2'} - F_2' - F_{2'}'\right)gb\mathrm{d}b\mathrm{d}\epsilon\mathrm{d}\mathbf{u}_{2'} \\ \rho_1\rho_2 I_{12}(K) &\equiv \iiint f_1^{(0)}f_2^{(0)}\left(K_{12} - K_{12}'\right)gb\mathrm{d}b\mathrm{d}\epsilon\mathrm{d}\mathbf{u}_2 \\ \rho_1\rho_2 I_{21}(K) &\equiv \iiint f_1^{(0)}f_2^{(0)}\left(K_{12} - K_{12}'\right)gb\mathrm{d}b\mathrm{d}\epsilon\mathrm{d}\mathbf{u}_1\end{aligned} \tag{0.24}$$

Note that $I_1(F)$ and $I_{12}(K)$ are functions of $\mathbf{u}_1$, while $I_2(F)$ and $I_{21}(K)$ are functions of $\mathbf{u}_2$. Further define the bracket integrals

$$[F, G]_i \equiv \int G_i I_i(F)\mathrm{d}\mathbf{u}_i, \qquad i = \{1, 2\} \tag{0.25}$$

For functions F and H defined on $\mathbf{u}_1$, and G and K defined on $\mathbf{u}_2$, define

$$[F_1 + G_2, H_1 + K_2]_{12} \equiv \int F_1 I_{12}(H_1 + K_2)\mathrm{d}\mathbf{u}_1 + \int G_2 I_{21}(H_1 + K_2)\mathrm{d}\mathbf{u}_2 \tag{0.26}$$

Expanding Equation (0.26), one quickly sees that $[F_1 + G_2, H_1 + K_2]_{12} = [H_1 + K_2, F_1 + G_2]_{12}$. Finally, for functions F and G both defined on $\mathbf{u}_1$ and $\mathbf{u}_2$, define the bracket integral

$$\rho^2\{F, G\} = \rho_1^2[F, G]_1 + \rho_1\rho_2[F_1 + F_2, G_1 + G_2]_{12} + \rho^2[F, G]_2. \tag{0.27}$$

Returning to the problem of determining the second approximation $f_1^{(1)} = f_1^{(0)}\Phi_1^{(1)}$, inserting Equations (0.23) and (0.21) into Equation (0.20) yields

$$\rho^2 I_1\left(\Phi_1^{(1)}\right) = -f_1^{(0)}\left[\left(\mathscr{U}_1{}^2 - \frac{5}{2}\right)\mathbf{U}_1\nabla\ln T + \frac{m}{k_B T}\boldsymbol{\mathscr{U}}_1\mathring{\boldsymbol{\mathscr{U}}}_1 : \nabla\mathbf{u}^n\right]. \tag{0.28}$$

Observe that $I_1\left(\Phi_1^{(1)}\right)$ is linear in $\Phi_1^{(1)}$, and that the right hand side of this equation is linear in the components of $\nabla\ln T$ and $\mathbf{u}^n$. Thereby, $\Phi_1^{(1)}$ can be written as a linear combination of the components of $\nabla\ln T$ and $\mathbf{u}^n$ and the solution to the equation $I_1\left(\Phi_1^{(1)}\right) = 0$. The latter can be recognised as a solution of the form in equation (0.14), such that for some vector $\mathbf{A}$, matrix $\underline{\boldsymbol{B}}$, and constants $\alpha^{(1,1)}, \boldsymbol{\alpha}^{(\mathbf{2,1})}, \alpha^{(3,1)}$

$$\Phi_1^{(1)} = -\frac{1}{\rho}\left(\frac{2k_B T}{m_1}\right)^{\frac{1}{2}}\mathbf{A}\nabla\ln T - \frac{2}{\rho}\underline{\boldsymbol{B}} : \nabla\mathbf{u}^n + \alpha^{(1,1)} + \boldsymbol{\alpha}^{(\mathbf{2,1})}m_1\mathbf{u}_1 + \alpha^{(3,1)}\frac{1}{2}m_1 U_1^2, \tag{0.29}$$

Where the prefactors to $\mathbf{A}$ and $\underline{\boldsymbol{B}}$ are chosen for later convenience. Substituting this into equation (0.28), using the fact that $I_1(F + G) = I_1(F) + I_1(G)$, and equating the coefficients to each of the gradient terms yields a set of equations for $\mathbf{A}$ and $\underline{\boldsymbol{B}}$,

$$\begin{aligned}\rho I_1(\mathbf{A}) &= f_1^{(0)}\left(\mathscr{U}_1{}^2 - \frac{5}{2}\right)\boldsymbol{\mathscr{U}} \\ \rho I_1(\underline{\boldsymbol{B}}) &= f_1^{(0)}\boldsymbol{\mathscr{U}}_1\mathring{\boldsymbol{\mathscr{U}}}_1.\end{aligned} \tag{0.30}$$

It is clear from the first of these equations that $\mathbf{A}$ must be a vector parallel to $\boldsymbol{\mathscr{U}}$, such that one can write

$$\mathbf{A} = A(\mathscr{U}, \rho, T)\boldsymbol{\mathscr{U}}, \tag{0.31}$$

where $\mathscr{U} \equiv |\boldsymbol{\mathscr{U}}|$ is the dimensionless peculiar speed. It is less clear, but can be shown, that $\underline{\boldsymbol{B}}$ is a symmetric, traceless matrix. All symmetric, traceless matrices that can be formed from $\boldsymbol{\mathscr{U}}$ are multiples of $\boldsymbol{\mathscr{U}}_1\mathring{\boldsymbol{\mathscr{U}}}_1$. Therefore, $\underline{\boldsymbol{B}}$ can be written as

$$\underline{\boldsymbol{B}} = B(\mathscr{U}, \rho, T)\boldsymbol{\mathscr{U}}_1\mathring{\boldsymbol{\mathscr{U}}}_1. \tag{0.32}$$

The constants $\alpha^{(1,1)}, \boldsymbol{\alpha}^{(\mathbf{2,1})}$ and $\alpha^{(3,1)}$ can be chosen such that $f_1^{(1)}$ satisfies the constraints posed by the summational invariants, from Equation (0.19). Analysing these constraints, one finds that $\alpha^{(1,1)} = \boldsymbol{\alpha}^{(\mathbf{2,1})} = \alpha^{(3,1)} = 0$ is a valid choice. Equation (0.29) then reduces to

$$\Phi_1^{(1)} = -\frac{1}{\rho_1}\left(\frac{2k_B T}{m_1}\right)^{\frac{1}{2}}\mathbf{A}\nabla\ln T - \frac{2}{\rho}\underline{\boldsymbol{B}} : \nabla\mathbf{u}^n. \tag{0.33}$$

Until now, for pedagogical reasons, only a simple gas has been considered. The method for arriving at Equation (0.33) for a binary system follows the exact same steps as those presented so far. Because the goal of this section is to describe diffusion, we now move to a binary case and in short words describe how the equation for $\Phi_1^{(1)}$ will differ from Equation (0.33).

0.1.4 The binary solutions

The Boltzmann equations for a binary system are directly analogous to that for a unary system,

$$\frac{\partial f_i}{\partial t} + \mathbf{u}\nabla f_i + \mathbf{F_i}\frac{\partial f_i}{\partial \mathbf{u}} = \frac{\partial_e f_i}{\partial t}, \qquad i = \{1, 2\}. \tag{0.34}$$

Rewriting this in terms of the operators $\mathscr{D}$ and J gives

$$\begin{aligned} \mathscr{D}_1 f_1 + J_1(f_1 f_{1'}) + J_{12}(f_1 f_2) = 0 \\ \mathscr{D}_2 f_2 + J_2(f_2 f_{2'}) + J_{21}(f_2 f_1) = 0 \end{aligned} \tag{0.35}$$

The subdivision of f_i and $\mathscr{D}_i$ follow the same procedure as the one outlined in the unary case. For J_i, the function $J_i^{(r)}$ takes the form

$$J_i^{(r)} \equiv \sum_{k=0}^{r} J_i(f_i^{(k)} f_{i'}^{(r-k)}) + J_{ij}(f_i^{(k)} f_j^{(r-k)}). \tag{0.36}$$

Again, requiring that $\mathscr{D}_i^{(r)} + J_i^{(r)} = 0 \ \forall \ r$ gives solutions to the first approximation identical to Equation (0.15). In the solution of the second approximation, a difference turns up. Inserting $f_1^{(1)} = f_1^{(0)}\Phi_1^{(1)}$ and $f_2^{(1)} = f_2^{(0)}\Phi_2^{(1)}$ into the expression for $J_1^{(1)}$ yields

$$J_1^{(1)} = \rho_1^2 I_1(\Phi_1^{(1)}) + \rho_1\rho_2 I_{12}(\Phi_1^{(1)} + \Phi_2^{(1)}). \tag{0.37}$$

Expanding $\mathscr{D}_1^{(1)}$ now yields

$$\mathscr{D}_1^{(1)} = f_1^{(0)}\left[\left(\boldsymbol{\mathscr{U}}_1 - \frac{5}{2}\right)\mathbf{U}_1\nabla\ln T + \frac{m}{k_B T}\boldsymbol{\mathscr{U}}_1\overset{\circ}{\boldsymbol{\mathscr{U}}}_1 : \nabla\mathbf{u}^n + x_1^{-1}\mathbf{d}_{12}\mathbf{U}_1\right] \tag{0.38}$$

Where the only difference from Equation (0.21) is the appearance of the trailing term

$$\mathbf{d}_{12} \equiv \nabla x_1 + \frac{\rho_1\rho_2(m_2 - m_1)}{\rho\rho_m}\nabla\ln p - \frac{\rho_{m,1}\rho_{m,2}}{\rho_m p}\left(\mathbf{F}_1 - \mathbf{F}_2\right), \tag{0.39}$$

where x_i denotes the mole fraction of species i, and ρ_m denotes the mass density. Just as in the previous section, it is now clear that $\Phi_1^{(1)}$ and $\Phi_2^{(1)}$ must be linear functions of $\nabla\ln T$, $\mathbf{d}_{12}$ and $\nabla\mathbf{u}^n$. Therefore, for some $\mathbf{A}$, $\mathbf{D}$ and $\underline{\boldsymbol{B}}$, the $\Phi_i^{(1)}$ may be written as

$$\Phi_i^{(1)} = -\mathbf{A}_i\nabla\ln T - \mathbf{D}_i\mathbf{d}_{12} - 2\underline{\boldsymbol{B}}_i : \nabla\mathbf{u}^n, \qquad i = \{1, 2\} \tag{0.40}$$

Inserting Equations (0.40) and (0.38) for $\Phi_i^{(1)}$ and $\mathscr{D}_i^{(1)}$ into Equations (0.35) and matching the coefficients of the gradients now leads to a set of equations that determine $\mathbf{A}$, $\mathbf{D}$ and $\underline{\boldsymbol{B}}$, analogous to Equations (0.30),

$$\begin{aligned} f_1^{(0)}(\boldsymbol{\mathscr{U}}_1^2 - \frac{5}{2})\mathbf{U}_1 &= \rho_1^2 I_1(\mathbf{A}_1) + \rho_1\rho_2 I_{12}(\mathbf{A}_1 + \mathbf{A}_2) \\ f_2^{(0)}(\boldsymbol{\mathscr{U}}_2^2 - \frac{5}{2})\mathbf{U}_2 &= \rho_2^2 I_2(\mathbf{A}_2) + \rho_2\rho_1 I_{21}(\mathbf{A}_2 + \mathbf{A}_1) \\ x_1^{-1} f_1^{(0)}\mathbf{U}_1 &= \rho_1^2 I_1(\mathbf{D}_1) + \rho_1\rho_2 I_{12}(\mathbf{D}_1 + \mathbf{D}_2) \\ -x_2^{-1} f_2^{(0)}\mathbf{U}_2 &= \rho_2^2 I_2(\mathbf{D}_2) + \rho_2\rho_1 I_{21}(\mathbf{D}_2 + \mathbf{D}_1) \\ f_1^{(0)}\boldsymbol{\mathscr{U}}_1\overset{\circ}{\boldsymbol{\mathscr{U}}}_1 &= \rho_1^2 I_1(\underline{\boldsymbol{B}}_1) + \rho_1\rho_2 I_{12}(\underline{\boldsymbol{B}}_1 + \underline{\boldsymbol{B}}_2) \\ f_2^{(0)}\boldsymbol{\mathscr{U}}_2\overset{\circ}{\boldsymbol{\mathscr{U}}}_2 &= \rho_2^2 I_2(\underline{\boldsymbol{B}}_2) + \rho_2\rho_1 I_{21}(\underline{\boldsymbol{B}}_2 + \underline{\boldsymbol{B}}_1) \end{aligned} \tag{0.41}$$

Thus, to a second approximation, the velocity distribution function is given as

$$\begin{aligned} f_i &= f_i^{(0)}(1+\Phi_i^{(1)}), \qquad i=\{1,2\} \\ &= f_i^{(0)}\left[1-\mathbf{A}_i\nabla\ln T-\mathbf{D}_i\mathbf{d}_{12}-2\underline{\boldsymbol{B}}_i:\nabla\mathbf{u}^n\right]. \end{aligned} \tag{0.42}$$

Note that $\mathbf{A}$, $\mathbf{D}$ and $\underline{\boldsymbol{B}}$ have been established to be unique, but determining their exact functional form still remains.

0.1.5 Diffusion

Now that an expression for the velocity distribution function has been obtained, the analysis of diffusion can begin. The two components of a mixture are diffusing relative to each other if $\bar{\mathbf{u}}_1-\bar{\mathbf{u}}_2\equiv\bar{\mathbf{U}}_1-\bar{\mathbf{U}}_2\neq 0$. Where the bar denotes the mean values of the velocity. From the velocity distribution function, the differences in mean velocity are

$$\bar{\mathbf{U}}_1-\bar{\mathbf{U}}_2=\frac{1}{\rho_1}\int f_1\mathbf{U}_1\mathrm{d}\mathbf{u}_1-\frac{1}{\rho_2}\int f_2\mathbf{U}_2\mathrm{d}\mathbf{u}_2. \tag{0.43}$$

Inserting the velocity distribution function from Equation (0.42), and noting that $f_i^{(0)}\mathbf{U}$, and $\underline{\boldsymbol{B}}_i:\nabla\mathbf{u}^n\mathbf{U}$ are odd functions such that their integrals vanish yields

$$\begin{aligned} \bar{\mathbf{U}}_1-\bar{\mathbf{U}}_2=-\frac{1}{3}\Bigg[&\left(\frac{1}{\rho_1}\int f_1^{(0)}\mathbf{U}_1\mathbf{D}_1\mathrm{d}\mathbf{u}_1-\frac{1}{\rho_2}\int f_2^{(0)}\mathbf{U}_2\mathbf{D}_2\mathrm{d}\mathbf{u}_2\right)\mathbf{d}_{12} \\ &+\left(\frac{1}{\rho_1}\int f_1^{(0)}\mathbf{U}_1\mathbf{A}_1\mathrm{d}\mathbf{u}_1-\frac{1}{\rho_2}\int f_2^{(0)}\mathbf{U}_2\mathbf{A}_2\mathrm{d}\mathbf{u}_2\right)\nabla\ln T\Bigg] \end{aligned} \tag{0.44}$$

Now, from Equations (0.41) it can be shown that for any vector function $\mathbf{a}$ defined on $\mathbf{u}_1$ and $\mathbf{u}_2$,

$$\begin{aligned} \rho^2\{\mathbf{A},\mathbf{a}\}&=\int f_1^{(0)}(\mathscr{U}_1^2-\frac{5}{2})\mathbf{U}_1\mathbf{a}_1\mathrm{d}\mathbf{u}_1+\int f_2^{(0)}(\mathscr{U}_2^2-\frac{5}{2})\mathbf{U}_2\mathbf{a}_2\mathrm{d}\mathbf{u}_2 \\ \rho^2\{\mathbf{D},\mathbf{a}\}&=x_1^{-1}\int f_1^{(0)}\mathbf{U}_1\mathbf{a}_1\mathrm{d}\mathbf{u}_1-x_2^{-1}\int f_2^{(0)}\mathbf{U}_2\mathbf{a}_2\mathrm{d}\mathbf{u}_2. \end{aligned} \tag{0.45}$$

Since $\mathbf{A}$ and $\mathbf{D}$ are exactly such vector functions, Equation (0.44) may be contracted to

$$\bar{\mathbf{U}}_1-\bar{\mathbf{U}}_2=-\frac{1}{3}\rho\left[\{\mathbf{D},\mathbf{D}\}\mathbf{d}_{12}+\{\mathbf{D},\mathbf{A}\}\nabla\ln T\right]. \tag{0.46}$$

Considering the cases in which either $\mathbf{d}_{12}=0$ or $\nabla T=\mathbf{F}_1=\mathbf{F}_2=\nabla p=0$ allows us to define the interdiffusion coefficient D_{12} and the thermal diffusion coefficient D_T for a binary mixture. In the first case,

$$\begin{aligned} \bar{\mathbf{u}}_1-\bar{\mathbf{u}}_2&=-\frac{\rho^2}{\rho_1\rho_2}D_T\nabla\ln T, \qquad \mathbf{d}_{12}=0 \\ &=-\frac{D_T}{x_1x_2}\nabla\ln T \\ D_T&\equiv\frac{\rho_1\rho_2}{3\rho}\{\mathbf{D},\mathbf{A}\} \end{aligned} \tag{0.47}$$

and in the second,

$$\begin{aligned} \bar{\mathbf{u}}_1-\bar{\mathbf{u}}_2&=-\frac{\rho^2}{\rho_1\rho_2}D_{12}\nabla x_1, \qquad \nabla T=\mathbf{F}_1=\mathbf{F}_2=\nabla p=0 \\ &=-\frac{D_{12}}{x_1x_2}\nabla x_1 \\ D_{12}&\equiv\frac{\rho_1\rho_2}{3\rho}\{\mathbf{D},\mathbf{D}\}. \end{aligned} \tag{0.48}$$

Additionally, the thermal diffusion ratio may be defined as

$$k_T \equiv \frac{D_T}{D_{12}} = \frac{\{\mathbf{D}, \mathbf{A}\}}{\{\mathbf{D}, \mathbf{D}\}} \tag{0.49}$$

To acquire values for the diffusion coefficients, it is thereby necessary to evaluate the integrals $\{\mathbf{D}, \mathbf{D}\}$ and $\{\mathbf{D}, \mathbf{A}\}$. To accomplish this, first introduce the auxiliary function $\tilde{\mathbf{A}}_i = \mathbf{A}_i - k_T \mathbf{D}_i$, then write the functions $\tilde{\mathbf{A}}_i$ and $\mathbf{D}_i$ as polynomial expansions using an orthogonal set of polynomials known as the Sonine polynomials, denoted $S_m^{(n)}(\varphi)$. These have the property

$$\int_0^\infty e^{-\varphi} S_m^{(p)}(\varphi) S_m^{(q)}(\varphi) \varphi^m d\varphi = \frac{\Gamma(m+p+1)}{p!} \delta_{pq} \tag{0.50}$$

where Γ denotes the gamma function and δ_{pq} is the Kronecker delta. $\mathbf{D}$ and $\tilde{\mathbf{A}}$ are expanded as

$$\mathbf{D}_1 = \sum_{p=-\infty}^{\infty} d_p \mathbf{a}_1^{(p)} \qquad \mathbf{D}_2 = \sum_{p=-\infty}^{\infty} d_p \mathbf{a}_2^{(p)} \tag{0.51}$$

$$\tilde{\mathbf{A}}_1 = \sum_{\substack{p=-\infty \\ p \neq 0}}^{\infty} a_p \mathbf{a}_1^{(p)} \qquad \tilde{\mathbf{A}}_2 = \sum_{\substack{p=-\infty \\ p \neq 0}}^{\infty} a_p \mathbf{a}_2^{(p)} \tag{0.52}$$

where

$$\mathbf{a}_1^{(p)} \equiv 0 \qquad \mathbf{a}_2^{(p)} \equiv S_{3/2}^{(p)}\left(\mathscr{U}_2^2\right) \boldsymbol{\mathscr{U}}_2 \qquad p < 0 \tag{0.53}$$

$$\mathbf{a}_1^{(0)} \equiv M_1^{\frac{1}{2}} \rho_{m,2} \rho_m^{-1} \boldsymbol{\mathscr{U}}_1 \qquad \mathbf{a}_2^{(0)} \equiv -M_2^{\frac{1}{2}} \rho_{m,1} \rho_m^{-1} \boldsymbol{\mathscr{U}}_2 \qquad p = 0 \tag{0.54}$$

$$\mathbf{a}_1^{(p)} \equiv S_{3/2}^{(p)}\left(\mathscr{U}_1^2\right) \boldsymbol{\mathscr{U}}_1 \qquad \mathbf{a}_2^{(p)} \equiv 0 \qquad p > 0 \tag{0.55}$$

Now, recall from Equation (0.45) that for any vector function $\mathbf{a}_i^{(p)}$, we may write

$$\rho^2 \{\mathbf{D}, \mathbf{a}^{(p)}\} = x_1^{-1} \int f_1^{(0)} \mathbf{U}_1 \mathbf{a}_1^{(p)} \mathrm{d}\mathbf{u}_1 - x_2^{-1} \int f_2^{(0)} \mathbf{U}_2 \mathbf{a}_2^{(p)} \mathrm{d}\mathbf{u}_2. \tag{0.56}$$

this integral can be evaluated analytically to give

$$\{\mathbf{D}, \mathbf{a}^{(p)}\} = \delta_p, \qquad \delta_p = \begin{cases} \frac{3}{2\rho} \left(\frac{2k_B T}{m_0}\right)^{\frac{1}{2}}, & p = 0 \\ 0, & p \neq 0, \end{cases}. \tag{0.57}$$

where $m_0 = m_1 + m_2$. Thus, by substituting the expansion of $\mathbf{D}$ from Equation (0.52), and utilising the orthogonality properties of the Sonine polynomials,

$$\sum_{p=-\infty}^{\infty} d_p \{\mathbf{a}^{(p)}, \mathbf{a}^{(q)}\} = \delta_q. \tag{0.58}$$

Exposing the integral $\{\tilde{\mathbf{A}}, \mathbf{a}^{(p)}\}$ to the same procedure yields

$$\sum_{\substack{p=-\infty \\ p \neq 0}}^{\infty} a_p \{\mathbf{a}^{(p)}, \mathbf{a}^{(q)}\} = \alpha_q, \qquad \alpha_q = \begin{cases} -\frac{15}{4} \frac{\rho_1}{\rho^2} \left(\frac{2k_B T}{m_1}\right)^{\frac{1}{2}} & q = 1 \\ 0 & q \neq \pm 1 \\ -\frac{15}{4} \frac{\rho_2}{\rho^2} \left(\frac{2k_B T}{m_2}\right)^{\frac{1}{2}} & q = -1 \end{cases} \tag{0.59}$$

These sets of linear equations uniquely determine the d_p and a_p, and thereby uniquely determine the functions $\mathbf{D}$, $\tilde{\mathbf{A}}$ and $\mathbf{A}$. For a finite approximation $|p| < N$, $|q| < N$, termed the Nth-order approximation, they may be written in matrix form as

$$\begin{bmatrix} a_{-N-N} & \dots & a_{-N0} & \dots & a_{-NN} \\ \vdots & \ddots & \vdots & & \vdots \\ a_{0-N} & \dots & a_{00} & \dots & a_{0N} \\ \vdots & & \vdots & \ddots & \vdots \\ a_{N-N} & \dots & a_{N0} & \dots & a_{NN} \end{bmatrix} \begin{pmatrix} d_{-N} \\ \vdots \\ d_0 \\ \vdots \\ d_N \end{pmatrix} = \begin{pmatrix} 0 \\ \vdots \\ 0 \\ \delta_0 \\ 0 \\ \vdots \\ 0 \end{pmatrix}, \tag{0.60}$$

$$\begin{bmatrix} a_{-N-N} & \dots & a_{-N-1} & a_{-N1} & \dots & a_{-NN} \\ \vdots & \ddots & \vdots & \vdots & & \vdots \\ a_{-1-N} & \dots & a_{-1-1} & a_{-11} & \dots & a_{-1N} \\ a_{1-N} & \dots & a_{1-1} & a_{11} & \dots & a_{1N} \\ \vdots & & \vdots & \vdots & \ddots & \vdots \\ a_{N-N} & \dots & a_{N-1} & a_{N1} & \dots & a_{NN} \end{bmatrix} \begin{pmatrix} a_{-N} \\ \vdots \\ a_{-1} \\ a_1 \\ \vdots \\ a_N \end{pmatrix} = \begin{pmatrix} 0 \\ \vdots \\ 0 \\ \alpha_{-1} \\ \alpha_1 \\ 0 \\ \vdots \\ 0 \end{pmatrix}, \tag{0.61}$$

Where $a_{pq} \equiv \{\mathbf{a}^{(p)}, \mathbf{a}^{(q)}\} = a_{qp}$. Further, inserting the expansions of $\mathbf{D}$ and $\tilde{\mathbf{A}}$ into the integrals $\{\mathbf{D}, \mathbf{D}\}$ and $\{\tilde{\mathbf{A}}, \tilde{\mathbf{A}}\}$ one arrives at

$$\{\mathbf{D}, \mathbf{D}\} = d_0\delta_0, \qquad \{\tilde{\mathbf{A}}, \tilde{\mathbf{A}}\} = a_1\alpha_1 + a_{-1}\alpha_{-1}, \qquad \{\mathbf{D}, \mathbf{A}\} = d_1\alpha_1 + d_{-1}\alpha_{-1}. \tag{0.62}$$

This means that evaluating the integrals a_{pq} is the final step to obtaining the diffusion coefficients. Recognise that when looking through all the nested notation that has been introduced, a_{pq} is simply the integral of two orthogonal polynomials. By all means, it is an octuple integral over six velocities and two collision parameters, but given an intermolecular potential it is essentially a number that can be evaluated (numerically if need be). The major issue is that the number of integrals that must be evaluated, and the complexity of these integrals, increases rapidly as one increases the order of approximation of $\mathbf{D}$ and $\mathbf{A}$, i.e. uses more polynomials in their expansions.

0.1.6 The summational expressions

To evaluate the integral $\{\mathbf{a}^{(p)}, \mathbf{a}^{(q)}\}$, Chapman and Cowling begin by inserting the definitions of $\mathbf{a}^{(p)}$ into the integral, and simplifying the expressions by using the orthogonality properties of the polynomials. This gives expressions for a_{pq} in terms of the square bracket integrals

$$\begin{aligned} a_{pq} &= x_1^2 \left[S_{3/2}^{(p)}(\mathscr{U}_1^2)\boldsymbol{\mathscr{U}}_1, S_{3/2}^{(q)}(\mathscr{U}_1^1)\boldsymbol{\mathscr{U}}_1 \right]_1 + x_1x_2 \left[S_{3/2}^{(p)}(\mathscr{U}_1^1)\boldsymbol{\mathscr{U}}_1, S_{3/2}^{(q)}(\mathscr{U}_1^2)\boldsymbol{\mathscr{U}}_1 \right]_{12} \\ a_{p-q} &= x_1x_2 \left[S_{3/2}^{(p)}(\mathscr{U}_1^2)\boldsymbol{\mathscr{U}}_1, S_{3/2}^{(q)}(\mathscr{U}_2^2)\boldsymbol{\mathscr{U}}_2 \right]_{12} \\ a_{-pq} &= x_1x_2 \left[S_{3/2}^{(p)}(\mathscr{U}_2^2)\boldsymbol{\mathscr{U}}_2, S_{3/2}^{(q)}(\mathscr{U}_1^2)\boldsymbol{\mathscr{U}}_1 \right]_{21} \\ a_{-p-q} &= x_2^2 \left[S_{3/2}^{(p)}(\mathscr{U}_2^2)\boldsymbol{\mathscr{U}}_2, S_{3/2}^{(q)}(\mathscr{U}_2^1)\boldsymbol{\mathscr{U}}_2 \right]_2 + x_1x_2 \left[S_{3/2}^{(p)}(\mathscr{U}_2^1)\boldsymbol{\mathscr{U}}_2, S_{3/2}^{(q)}(\mathscr{U}_2^2)\boldsymbol{\mathscr{U}}_2 \right]_{21}. \end{aligned} \tag{0.63}$$

It is noted from the symmetry properties of the square bracket integrals that only the evaluation of

$$\begin{aligned} H_1^{(1)}(p,q) &\equiv \left[S_{3/2}^{(p)}(\mathscr{U}_1^2)\boldsymbol{\mathscr{U}}_1, S_{3/2}^{(q)}(\mathscr{U}_1^1)\boldsymbol{\mathscr{U}}_1\right]_1 \\ H_{12}^{(1)}(p,q) &\equiv \left[S_{3/2}^{(p)}(\mathscr{U}_1^1)\boldsymbol{\mathscr{U}}_1, S_{3/2}^{(q)}(\mathscr{U}_1^2)\boldsymbol{\mathscr{U}}_1\right]_{12} \\ H_{12}^{(12)}(p,q) &\equiv \left[S_{3/2}^{(p)}(\mathscr{U}_1^2)\boldsymbol{\mathscr{U}}_1, S_{3/2}^{(q)}(\mathscr{U}_2^2)\boldsymbol{\mathscr{U}}_2\right]_{12} \end{aligned} \tag{0.64}$$

is required, and the rest can be obtained by index swapping. Recognise now that all information about the intermolecular potential is contained in the integral over $\mathrm{d}b\mathrm{d}\epsilon$, while the integrals over velocity may be carried out without specifying any such potential. It is therefore convenient to define the *collision integrals* $\Omega_{12}^{(\ell)}(r)$ and $\Omega_i^{(\ell)}(r)$, $i = \{1,2\}$

$$\begin{aligned} \Omega_{12}^{(\ell)}(r) &\equiv \frac{1}{2}\sigma_1 2^2 \left(\frac{k_B T}{2\pi m_0 M_1 M_2}\right)^{\frac{1}{2}} W_{12}^{(\ell)}(r) \\ W_{12}^{(\ell)}(r) &\equiv \int_0^\infty \exp(-\mathfrak{g}^2)\mathfrak{g}^{2r+3} \int_0^\pi \left(1-\cos^l(\chi)\right)\left(\frac{b}{\sigma_{12}}\right) d\left(\frac{b}{\sigma_{12}}\right) d\mathfrak{g}_{21} \end{aligned} \tag{0.65}$$

where $\mathfrak{g}_{21} = \left(\frac{m_0 M_1 M_2}{2k_B T}\right)^{\frac{1}{2}} \mathbf{g_{21}}$ is the non-dimensional relative velocity, and a change of integration variables has been employed to map $\mathrm{d}b\mathrm{d}\epsilon \mapsto d\left(\frac{b}{\sigma_{12}}\right) d\mathfrak{g}_{21}$. The equivalent expression for $\Omega_i^{(\ell)}(r)$ is

$$\Omega_i^{(\ell)}(r) \equiv \sigma_i^2 \left(\frac{\pi k_B T}{m_1}\right)^{\frac{1}{2}} W_i^{(\ell)}(r), \qquad i = \{1,2\} \tag{0.66}$$

where $W_i^{(\ell)}(r)$ is obtained simply by replacing σ_{12} with σ_i in Equation (0.65). The collision integrals can be evaluated numerically for any given intermolecular potential, by using this potential to relate χ to b and $\mathfrak{g}$, as described in detail by Chapman and Cowling pp. 167.[1] In addition, Reid et al. give several methods of approximating the collision integrals under various conditions.[4] However, for a HS-potential the integrals can be evaluated analytically to give

$$\begin{aligned} \Omega_1^{(\ell),HS}(r) &= (\sigma_1^{HS})^2 \left(\frac{\pi k_B T}{m_1}\right)^{\frac{1}{2}} W_r^{(\ell),HS} \\ \Omega_2^{(\ell),HS}(r) &= (\sigma_2^{HS})^2 \left(\frac{\pi k_B T}{m_2}\right)^{\frac{1}{2}} W_r^{(\ell),HS} \\ \Omega_{12}^{(\ell),HS}(r) &= \frac{1}{2}(\sigma_{12}^{HS})^2 \left(\frac{2\pi k_B T}{m_0 M_1 M_2}\right)^{\frac{1}{2}} W_r^{(\ell),HS} \\ W_r^{(\ell),HS} &= \frac{1}{4}\left[2 - \frac{1}{l+1}\left(1+(-1)^l\right)\right](r+1)!. \end{aligned} \tag{0.67}$$

Having defined the collision integrals, Chapman and Cowling expand the integrals over $\mathbf{u}_1$ and $\mathbf{u}_2$ and determine that the complete integrals may be written as linear combinations of the collision integrals,

$$\begin{aligned} H_1^{(1)}(p,q) &= 8 \sum_{l=2}^{(\min[p,q]+1)} \sum_{r=l}^{(p+q+2-\ell)} A'''_{pqr\ell}\Omega_1^{(\ell)}(r) \\ H_{12}^{(1)}(p,q) &= 8 \sum_{l=1}^{(\min[p,q]+1)} \sum_{r=l}^{(p+q+2-\ell)} A'_{pqr\ell}\Omega_{12}^{(\ell)}(r) \\ H_{12}^{(12)}(p,q) &= 8M_2^{(p+\frac{1}{2})}M_1^{(q+\frac{1}{2})} \sum_{l=1}^{(\min[p,q]+1)} \sum_{r=l}^{(p+q+2-l)} A_{pqr\ell}\Omega_{12}^{(\ell)}(r) \end{aligned} \tag{0.68}$$

with $A_{pqr\ell}$, $A'''_{pqr\ell}$ as yet undetermined weights, independent of any molecular properties. $A'_{pqr\ell}$ is an undetermined number that is a function of the particle masses. Identifying explicit expressions for these weights is an abnormally extensive exercise in analytical integration and pattern matching that was carried out by Thompson et al.[5–8] For the derivation the reader is referred to their papers. The results they give are

$$\begin{aligned} A'''_{pqr\ell} = \left(\frac{1}{2}\right)^{(p+q+1)} & \sum_{i=(l-1)}^{(\min[p,q,r,(p+q+1-r)])} \frac{8^i (p+q-2i)!\left(1+(-1)^l\right)}{(p-i)!(q-i)!(\ell)!(i+1-l)!} \\ & \times \frac{(-1)^{(r+i)}(r+1)!(2(p+q+2-i))!2^{2r}}{(r-i)!(p+q+1-i-r)!(2r+2)!(p+q+2-i)!4^{(p+q+1)}} \\ & \times [(i+1-l)(p+q+1-i-r)-\ell(r-i)] \end{aligned} \tag{0.69}$$

$$\begin{aligned} A'_{pqr\ell} = & \sum_{i=(l-1)}^{\min[p,q,r,(p+q+1-r)]} \sum_{k=(l-1)}^{\min[l,i]} \sum_{w=0}^{(\min[p,q,(p+q+1-r)]-i)} \frac{8^i (p+q-2i-w)!}{(p-i-w)!(q-i-w)!} \\ & \times \frac{(-1)^{(r+i)}(r+1)!(2(p+q+2-i-w))!4^{(r+w)}F^{(i+k)}G^w M_1^i M_2^{(p+q-i-w)}}{(r-i)!(p+q+1-i-r-w)!(2r+2)!(p+q+2-i-w)!4^{(p+q+1)}(k)!(i-k)!(w)!} \\ & \times \left(M_1(p+q+1-i-r-w)\delta_{k,l} - M_2(r-i)\delta_{k,(l-1)}\right) \\ & F \equiv \frac{M_1^2+M_2^2}{M_1 M_2}, \qquad G \equiv \frac{M_1-M_2}{M_2} \end{aligned} \tag{0.70}$$

$$\begin{aligned} A_{pqr\ell} = & \sum_{i=(l-1)}^{\min[p,q,r,(p+q+1-r)]} \frac{8^i (p+q-2i)!}{(p-i)!(q-i)!(\ell)!(i+1-l)!(r-i)!} \\ & \times \frac{(-1)^{(l+r+i)}(r+1)!(2(p+q+2-i))!4^r}{(p+q+1-i-r)!(2r+2)!(p+q+2-i)!4^{(p+q+1)}} \\ & \times [(i+1-l)(p+q+1-i-r)-\ell(r-i)] \end{aligned} \tag{0.71}$$

These three factors will later be collectively referred to as the "A_{pqrl} factors".

0.1.7 Summary

Though the derivation outlined above is quite lengthy, notice that the implementation of the final result is almost trivial once one understands the significance of each variable. With explicit expressions for the $A_{pqr\ell}$, $A'_{pqr\ell}$ and $A'''_{pqr\ell}$, the evaluation of the linear combinations in Equation (0.68) for a given (p,q) is straight forward. Once these are evaluated, the corresponding a_{pq} matrix element in the linear set of equations (0.61) have been determined. To compute the diffusion coefficients at a given order of approximation N, all the a_{pq}, $(p,q) \in (-N,N) \times (-NN)$, matrix elements must be computed such that the matrix equation (0.61) can be solved to obtain the d_{-1}, d_0 and d_1.

1 Methods

1.1 The Enskog solutions

As indicated in Section 0.1.7, implementation of the Enskog solutions using the explicit summational expressions obtained by Tompson et al. is straight forward. A practical issue of note is that the factorial operations in the sums defining the A_{pqrl} factors tend to cause overflow issues already at quite low orders of approximation. Already at order $N = 5$, the factorial 24! must be evaluated, which is too large for a 64-bit unsigned

integer. To remedy this, it was noted that although there are very large numbers involved in the evaluation of the A_{pqrl}-factors, they largely cancel in the fractions. Therefore, a "smart" evaluation of factorials and fractions was implemented. The implementation defines data types for factorials, products and fractions with the multiplication and division operator defined such that fractions containing products of integers and factorials can be exactly represented. This is done by treating a product as a list of integers, and a fraction as two products; the numerator and the denominator. If a product is multiplied by a non-integer type, the non-integer part of the product is stored separately. The actual evaluation of the products is not done until explicitly required. Upon evaluation of the fractions, common integers in the numerator and denominator are cancelled, then the simplified numerator and denominator are evaluated and the results divided by each other, much like one would do the computation manually. This was tested up to approximation order $N = 25$ and prevented overflow up to that order.

Another practical question of interest is what potential and parameters one should use for the collision integrals. In this work, the hard-sphere collision integrals were implemented, using two different approaches to obtain the hard-sphere diameters. The first approach simply uses Mie-potential σ-parameters. The argument for this is that the Mie-potential rises very steeply, behaving almost like a hard sphere potential, at $r < \sigma$. Therefore, σ should be a reasonable first approximation to the shortest possible distance between the centre of mass of two particles. The second approach employs the Barker-Henderson (BH) diameter (d_{BH}) defined as

$$d_{BH} = \int_0^\sigma 1 - \exp\left(-\frac{u^{Mie}(r)}{k_B T}\right) dr \tag{1.1}$$

where u^{Mie} is the Mie potential,

$$u^{Mie}(r) = C\varepsilon\left[\left(\frac{\sigma}{r}\right)^{\lambda_r} - \left(\frac{\sigma}{r}\right)^{\lambda_a}\right], \qquad C = \frac{\lambda_r}{\lambda_r - \lambda_a}\left(\frac{\lambda_r}{\lambda_a}\right)^{\frac{\lambda_a}{\lambda_r - \lambda_a}}. \tag{1.2}$$

Here, λ_r and λ_a are the repulsive and attractive exponents. The specific case $\lambda_r = 12$, $\lambda_a = 6$ is the commonly known Lennard-Jones (LJ) potential or the LJ (12-6) potential.

The BH-diameter is very close to the σ-parameter at low temperatures but decreases with increasing temperature, as shown in Figure 1.1. This simulates the fact that particles moving at a higher velocity (higher temperature) will come closer together before deflecting. In a sense, this can be thought of as a rough manner of approximating the effect one would see if the collision integrals were implemented using a purely repulsive potential similar to the repulsive part of the Mie-potential. The difference in these two approaches is investigated in Section 2.1, and discussed further in Section **??**.

Finally, the convergence of the Enskog solutions with increasing order of approximation was investigated. As shown in Figure 1.2, the coefficients d_{-1}, d_0 and d_1 converge already at the fourth or fifth order approximation. A fifth order approximation was used to generate the results presented in Sections **??**, **??** and **??**. In the making of this report it was recognised that the thermal diffusion ratio predicted at higher order approximations ($N > 7$) was divergent under certain conditions. This is investigated and discussed in closer detail in Section 2.2.

The final implementation of the Enskog solutions used in this work can be found in a public repository on GitHub.[9]

1.1.1 Numerical error

In the study of the higher order Enskog solutions, the effect and magnitude of the numerical error introduced in the solution of Equation (0.60), which yields the expansion coefficients d_{-1}, d_0 and d_1, was investigated. To do this, a meaningful manner in which to measure the error in the matrix inversion must be identified. For convenience of notation, Equation (0.60) may be written as

$$\underline{\boldsymbol{D}}_N \left[\mathbf{d}\right]_N = \boldsymbol{\delta}, \tag{1.3}$$

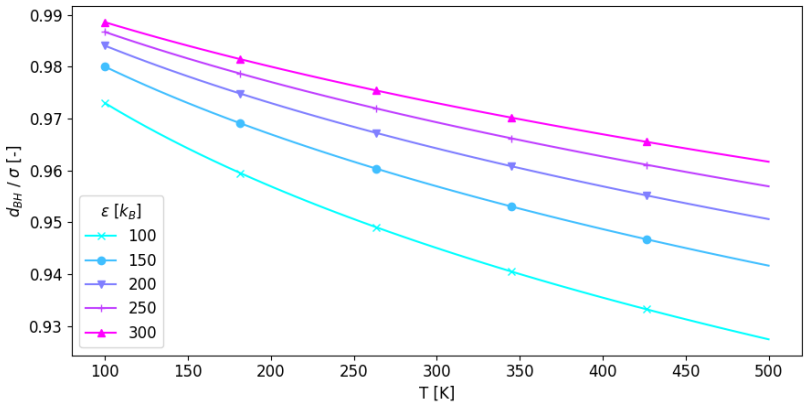

Figure 1.1: Ratio of the BH-diameter to the σ-parameter of the Lennard-Jones 12-6 potential as a function of temperature, for different ε-values. The ratio is not a function of the σ-parameter, as can be shown by differentiating Equation (1.1).

where $[\mathbf{d}]_N$, is the exact Nth approximation to the vector of Sonine polynomial expansion coefficients, devoid of numerical error and $\underline{\boldsymbol{D}}_N$ is the matrix containing some truncation error from the evaluation of the a_{pq} elements. $\boldsymbol{\delta}$ is the vector of all zeros, except the central element $\delta_{0,\tilde{}}$ which is a float value with inherent truncation error. The numerical solution to Equation (1.3) is denoted $[\mathbf{d}]_N$. A simple manner of investigating the expected error introduced when inverting $\underline{\boldsymbol{D}}_N$ is computing the condition number, $\kappa(\underline{\boldsymbol{D}}_N)$. This number gives an indication of how much a change in $\underline{\boldsymbol{D}}_N$ or $\boldsymbol{\delta}$ will effect the solution to the equation, i.e. how sensitive it is to float truncation error. A large condition number indicates an ill-conditioned problem, with high potential error. The remainder of this section presents an alternative measure for the deviation of the numerical solution from the true solution.

Assuming that the numerical error introduced in the evaluation of the a_{pq} matrix elements is negligible, all error in $[\tilde{\mathbf{d}}]_N$ stems from the matrix inversion. This is likely a reasonable assumption, because the implemented "smart" evaluation of the A_{pqrl} factors simplifies all fractions in Equations (0.69) to (0.71) by an exact method before evaluation. This reduces the absolute value of the numerator and denominator such that float truncation error becomes less significant. Now, upon numerically inverting the matrix $\underline{\boldsymbol{D}}_N$, assume that some error ϵ is introduced, such that

$$\begin{aligned}[\mathbf{d}]_N &= [\tilde{\mathbf{d}}]_N + \boldsymbol{\epsilon} \\ &= \underline{\boldsymbol{D}}_N^{-1}\boldsymbol{\delta} + \boldsymbol{\epsilon}.\end{aligned} \tag{1.4}$$

Further, because Equation (1.3) is assumed to hold exactly, left-multiplication by $\underline{\boldsymbol{D}}_N$ yields

$$\begin{aligned}\boldsymbol{\delta} &= \underline{\boldsymbol{D}}_N\underline{\boldsymbol{D}}_N^{-1}\boldsymbol{\delta} + \underline{\boldsymbol{D}}_N\boldsymbol{\epsilon} \\ \underline{\boldsymbol{D}}_N\boldsymbol{\epsilon} &= \left(\underline{\boldsymbol{I}} - \underline{\boldsymbol{D}}_N\underline{\boldsymbol{D}}_N^{-1}\right)\boldsymbol{\delta}\end{aligned} \tag{1.5}$$

where $\underline{\boldsymbol{I}}$ is the identity matrix. This obviously holds, as the factor in the parentheses on the right hand side is identically zero if there is no error in the matrix inversion. Left-multiplying by $\underline{\boldsymbol{D}}_N^{-1}$ gives

$$\boldsymbol{\epsilon} = \underline{\boldsymbol{D}}_N^{-1}\left(\underline{\boldsymbol{I}} - \underline{\boldsymbol{D}}_N\underline{\boldsymbol{D}}_N^{-1}\right)\boldsymbol{\delta} + \boldsymbol{\epsilon}' \tag{1.6}$$

Neglecting the error introduced in this operation, $\boldsymbol{\epsilon}'$, then gives

$$\boldsymbol{\epsilon} \approx \underline{\boldsymbol{D}}_N^{-1}\left(\underline{\boldsymbol{I}} - \underline{\boldsymbol{D}}_N\underline{\boldsymbol{D}}_N^{-1}\right)\boldsymbol{\delta}. \tag{1.7}$$

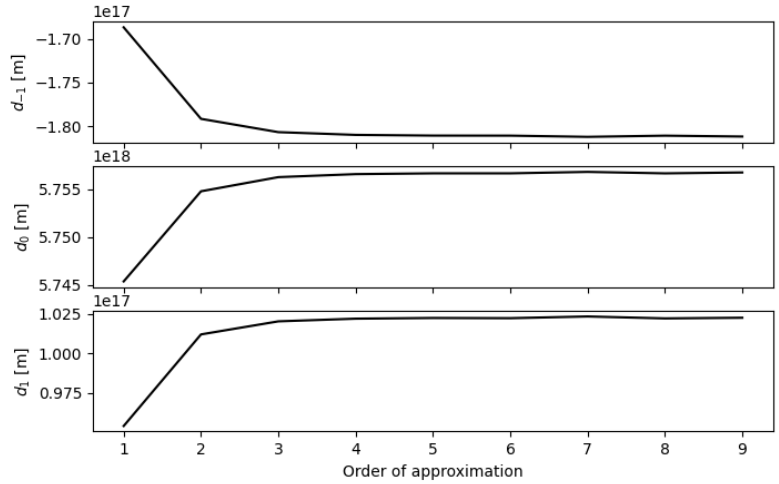

Figure 1.2: Convergence of the computed d_{-1}, d_0 and d_1 with increasing order of approximation. Using $m_1 = 15\,\mathrm{g\,mol^{-1}}$, $m_2 = 10\,\mathrm{g\,mol^{-1}}$, $\sigma_1 = 1.5$ Å, $\sigma_2 = 2$ Å and $\sigma_{12} = 1.75$ Å, with a hard-sphere potential for the collision integrals.

Finally, because it is the error in the three components d_{-1}, d_0 and d_1 that is of interest, and the value of $[\mathbf{d}]_N$ is a function of particle masses, HS-diameters and composition, define the relative error

$$\epsilon_N^r \equiv \left| \frac{\epsilon_{-1}}{[d_{-1}]_N} \right| + \left| \frac{\epsilon_0}{[d_0]_N} \right| + \left| \frac{\epsilon_1}{[d_1]_N} \right|. \tag{1.8}$$

When interpreting the value of ϵ_N^r, note that floating point precision in the computations in this work is 10^{-16}, so a relative error on the order of $10^{-16} - 10^{-14}$ indicates that no error beyond that inherent to floating point arithmetic has been introduced in the matrix inversion.

2 Results

2.1 Analysis of the Enskog diffusion solutions

The implemented module for solution of the Boltzmann equations was tested to confirm the absence of implementation errors. This was also used as an opportunity to investigate the behaviour of the solutions at different orders of approximation, and the solutions dependencies on the various parameters. The validation was done by comparing predicted diffusion coefficients to those predicted by the Fuller diffusion model.[10] This model is based on empirical fitting of the exponents in the expression resulting from the first Enskog approximation. That is,

$$[D_{12}]_1 = \frac{3}{32\rho\sigma_{12}^2}\left[\frac{8k_BT}{\pi}\left(\frac{1}{m_1}+\frac{1}{m_2}\right)\right]^{\frac{1}{2}} \tag{2.1}$$

where the equation subject to the regression is

$$D_{12} = \frac{AT^b\left(\frac{1}{m_1}+\frac{1}{m_2}\right)^{\frac{1}{2}}}{p\left[\left(\sum_i \upsilon_{1,i}\right)^{\alpha_1}+\left(\sum_i \upsilon_{2,i}\right)^{\alpha_2}\right]^{\alpha_3}}. \tag{2.2}$$

The results of the regression presented by Fuller are shown in Table 2.1.

Table 2.1: Parameters used in Fuller-diffusion model.[10] Diffusion volumes are summed over groups of atoms in each molecule, except in the case of monoatomic species.

Parameter	Description	Value
A	Constant for all mixtures	$0.1\,\mathrm{s\,m^{-1}\,K^{-1.75}}$
b	Temperature exponent	1.75
α_1, α_2	Diffusion volume exponents	$\frac{1}{3}$
α_3	Total volume exponent	2
$\sum_i \upsilon_{1,i}$	Diffusion volume of species 1	$(16.1\,\mathrm{mL})^*$
$\sum_i \upsilon_{2,i}$	Diffusion volume of species 2	$(2.88\,\mathrm{mL})^{**}$

*Argon
**Helium

Because the Fuller-diffusion model is the result of fitting against a large set of empirical data, replication of the predictions by this model is closely analogous to replicating those data. As seen in Figure 2.1a, Enskog theory predicts a too weak temperature dependency of the diffusion coefficient ($D_{12} \sim T^{\frac{3}{2}}$, dashed lines). This was also noted by Fuller, and was his reasoning for fitting the temperature exponent. Using the temperature-dependent BH-diameter, as described in Section 1.1, gives a better fit to the Fuller-model. When using the BH-diameters, the temperature dependency was determined to $D_{12} \sim T^{1.6}$ by a simple regression on the function $D_{12} = aT^b$. Enskog theory predicts the diffusion coefficient to vanish at absolute zero, removing the need for a constant term in the regression. It is also clear that the difference between the 1st and 5th order Enskog approximations are minimal at these conditions.

The Fuller diffusion model does not predict a compositional dependency of the interdiffusion-coefficient. As seen in Figure 2.1b, this coincides with the predictions of the 1st-order Enskog approximation, upon which the Fuller-model is based. It may seem unreasonable that the 1st-order approximation gives the same prediction as the higher-order approximations in the limit of infinite dilution of one component but not the other. A closer investigation shows that in mixtures with large mass ratios, the diffusion coefficient will approach the 1st-order diffusion coefficient in the limit of infinite dilution of the heavier component, as shown in Figure 2.2a. Varying the ratio of the HS-diameters also produces results that are symmetrical about $x_1 = x_2 = 0.5$, as shown in Figure 2.2b.

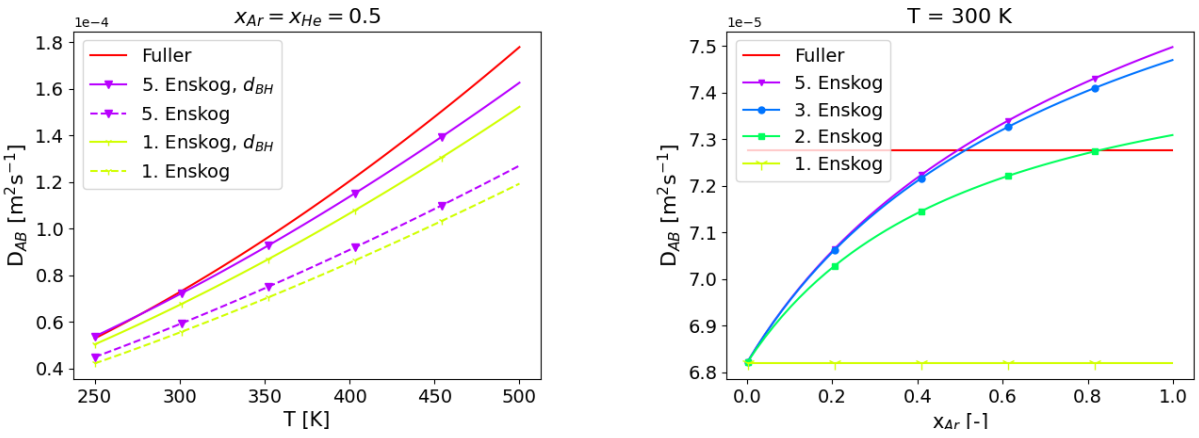

(a)

(b) All predictions with d_{BH}.

Figure 2.1: Predicted diffusion coefficients by Enskog-theory, with and without temperature dependent hard-sphere diameters, and the Fuller diffusion model. d_{BH} indicates predictions using BH-diameters. The diffusion coefficient predicted using BH-diameters has a temperature dependency of $D_{12} \sim T^{1.6}$, determined by regression.

Finally, the predicted pressure dependency of the diffusion coefficients was investigated. Note that the pressure dependency in the equation subject to the regression is only equivalent to that of Enskog theory for an ideal gas, where $\frac{n}{V} \propto p$, as the expression derived from Kinetic gas theory is explicit in density rather than pressure. The predicted pressure dependency of the diffusion coefficient therefore depends on the EoS chosen to translate between pressure and density. Using the ideal gas law, the results are as shown in Figure 2.3.

Using the 1st-order approximation obviously gives the same pressure dependency as the Fuller-model when using the ideal gas law to compute the mixture density. It is however, worth noting that no additional pressure dependency appears when increasing the order of approximation, as is the case with the compositional dependency.

In summary, the implementation of the Enskog solutions performs as expected. That is, the temperature dependency of the diffusion coefficient is weaker that that which is observed experimentally and there is no compositional dependency in the first order approximation. Additionally, the pressure dependency is identical to that reported by Fuller, which is expected for the first order approximation, as Fuller did not have the pressure exponent as a free variable in the fitting of the Fuller diffusion model. Lastly, using BH-diameters improved the agreement between the Enskog solutions and the Fuller diffusion model. As argued in Section 1.1, the use of BH-diameters is a rough manner in which to approximate the effect of using a more realistic potential in the collision integrals. It was therefore expected that this would improve the agreement with the Fuller model regarding temperature dependency.

Regarding the higher order approximations there are some properties worth noting. The diffusion coefficients dependency on pressure and temperature (when not using BH-diameters) are completely contained in the 1st approximation, while the compositional dependency is contained in the higher order solutions. Mathematically, this has its roots in the fact that the entire density dependence of the diffusion solutions are contained in δ_0 in Equation (0.60), while the compositional dependency is included in every element a_{pq} of the matrix in the same equation. Likewise, the temperature dependency can be factored out of the matrix, meaning that no new temperature dependency is included upon increasing the order of approximation. The latter is shown by recognising the a_{pq} matrix elements as linear combinations of the collision integrals, which all have the same temperature dependence.

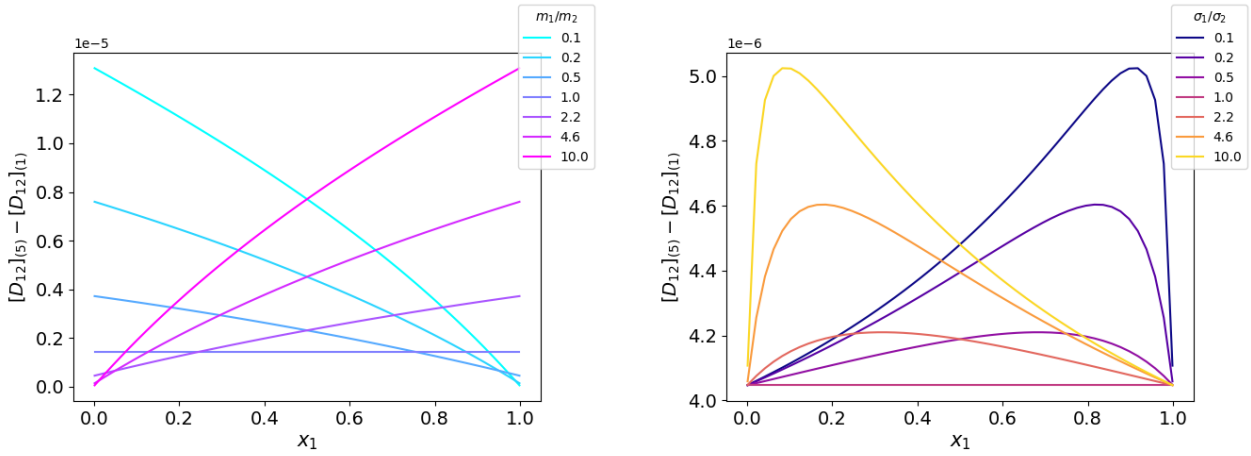

(a) Varying $\frac{m_1}{m_2}$

(b) Varying $\frac{\sigma_1}{\sigma_2}$

Figure 2.2: Compositional dependency of the interdiffusion coefficient at different mass- and hard sphere diameter ratios. In both cases the average value (mass or diameter) is kept constant and equal to $5\,\mathrm{g\,mol^{-1}}$ and 3.405 Å respectively.

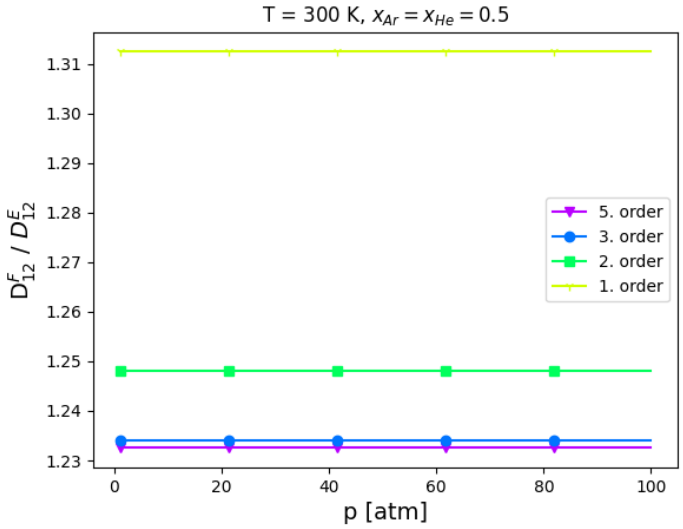

Figure 2.3: Ratio of Fuller-model to Enskog-theory diffusion coefficient, at different order of approximation, with varying pressure. Density computed from ideal gas law.

2.2 Model divergence

Both the Kempers-model and the Enskog solutions displayed divergent behaviour under certain conditions. This section investigates the behaviour with the intent of making clear why it is observed and if there may be a physical interpretation of the divergent solutions.

The Kempers-model was shown to diverge for a certain temperature, density and composition. From the model for a binary system, Equation (**??**), it is clear that the model will diverge when $\left(\frac{\partial \mu_i}{\partial x_j}\right)_{T,p,n_k} = 0$. This corresponds to an inflection point in the Gibbs energy as a function of composition, indicating that the mixture is thermodynamically unstable. The divergence of the thermodynamic contribution can thereby be understood as a physically sound solution rather than a failure of the model. Disregarding the kinetics, mixture at the composition of divergence will tend to separate, creating a phase boundary. At the interface between two stable phases of different composition, the Soret coefficient, as defined in Equation (**??**), is necessarily divergent, as the compositional gradient will remain nonzero even as the thermal gradient vanishes. The question of whether a meaningful definition of the Soret coefficient at the interface can be obtained is left untouched in this work.

It was observed that the implementation of the Enskog solutions produced a divergent thermal diffusion ratio for certain compositions at higher order approximations, hence the use of 5th order approximations for all figures unless otherwise is explicitly stated. In one case, shown in Figure **??** at approximately $w_{\mathrm{EtOH}} = 0.82$, the divergence was observed at order 5. Initially it was thought that this may be the manifestation of some higher order effect, as the composition at which the thermal diffusion ratio diverged varied from system to system. The Carnahan-Starling hard-sphere EoS is known to be capable of predicting phase transitions,[11] and the thought that higher order approximations to the Enskog solutions could do the same was entertained. However, no indication of this was found in the literature.

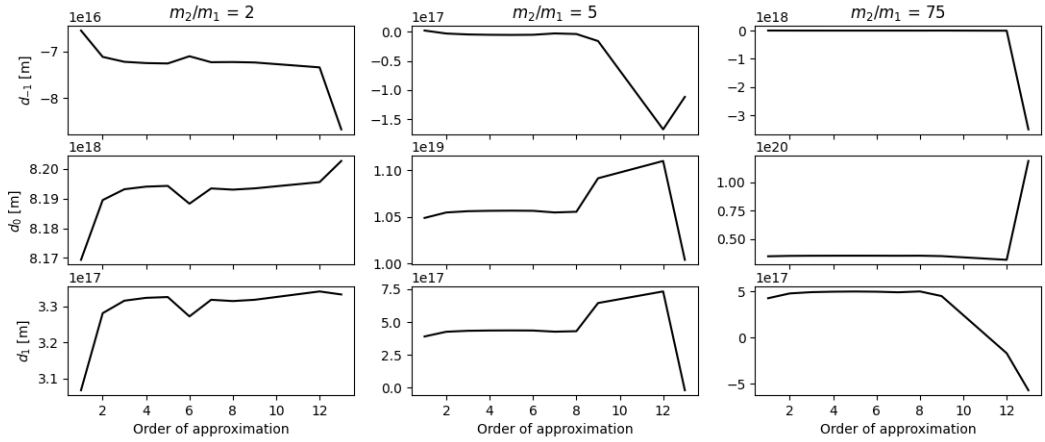

Figure 2.4: The expansion coefficients of the diffusion function **D** obtained from the Enskog solutions at different orders of approximation, with varying mass ratios. The value of parameters that were not varied are displayed in Table 2.2.

In order to investigate the divergence more closely, the expansion coefficients d_{-1}, d_0 and d_1 obtained from Equation (0.60) were computed at various orders of approximation while individually varying the hard sphere diameter ratio, the mass ratio and the composition. Note that the interdiffusion coefficient is proportional to d_0, while the thermal diffusion coefficient is proportional to d_{-1} and d_1. As shown in Figure 2.4, there is a small instability at $N = 6$ for a mass ratio of $m_2/m_1 = 2$, but the solution stabilises again until $N = 12$. Increasing the mass ratio led the solutions to become unstable at lower order approximations, with the instability kicking in at $N = 8$. Further increasing the mass ratio led the solutions to diverge more severely,

but not earlier than at $N = 7$. This was tested for mass ratios gradually increasing up to 75, with ratios of 2, 15 and 75 shown in Figure 2.4. In none of the cases did the solutions appear to stabilise at some new value when increasing the order of approximation, even up to $N = 20$.

Further, the HS-diameter ratios were systematically varied, but as shown in Figure 2.5, this does not appear to have any effect on the stability of the solutions. Finally, varying the composition at a constant mass ratio $m_2/m_1 = 2$ was tested. It appears that the solutions become stable at higher order approximations as the mole fraction of the lighter component is increased, as shown in Figure 2.6.

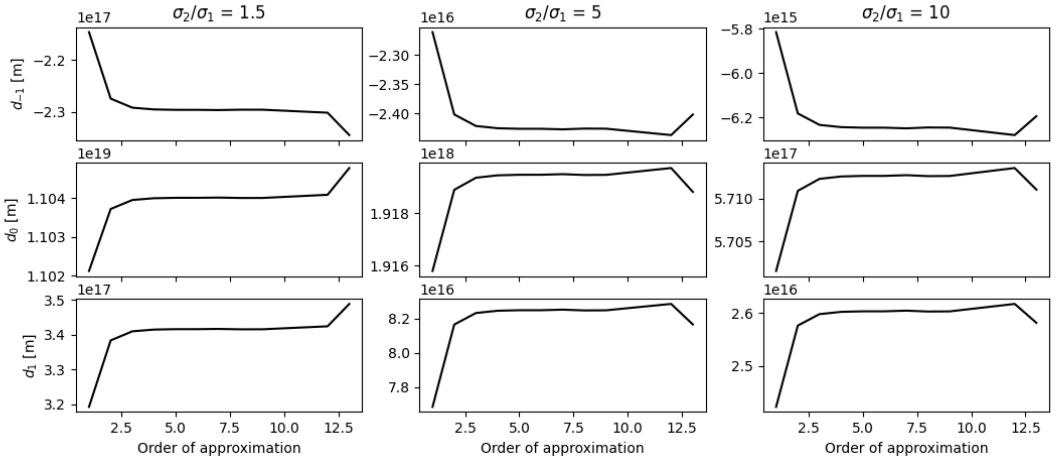

Figure 2.5: The expansion coefficients of the diffusion function **D** obtained from the Enskog solutions at different orders of approximation, at various HS-diameter ratios. The value of parameters that were not varied are displayed in Table 2.2.

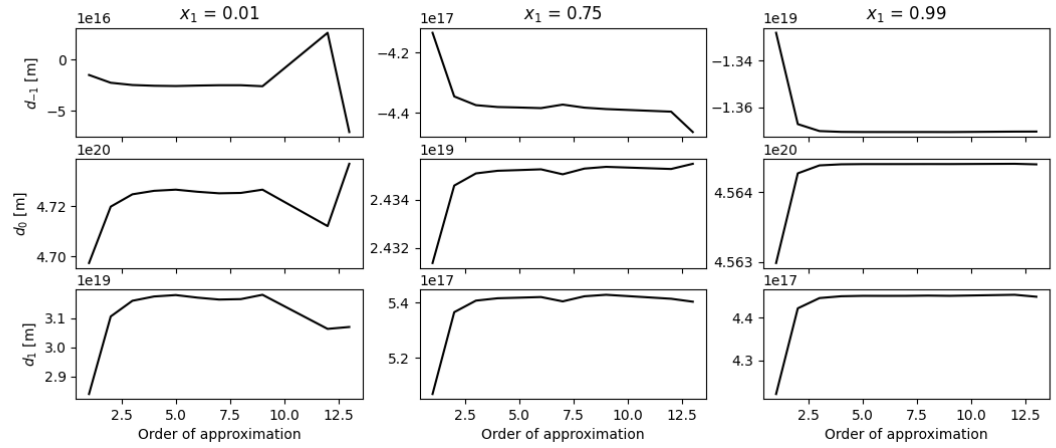

Figure 2.6: The expansion coefficients of the diffusion function **D** obtained from the Enskog solutions at different orders of approximation, at various compositions. The value of parameters that were not varied are displayed in Table 2.2.

Though these results shed some light on what conditions the Enskog solutions destabilise under, no immediate physical explanation for the instability reveals itself. Therefore, the error introduced in the numerical inversion of the matrix in Equation (0.60) was analysed by the methods described in Section 1.1.1. First

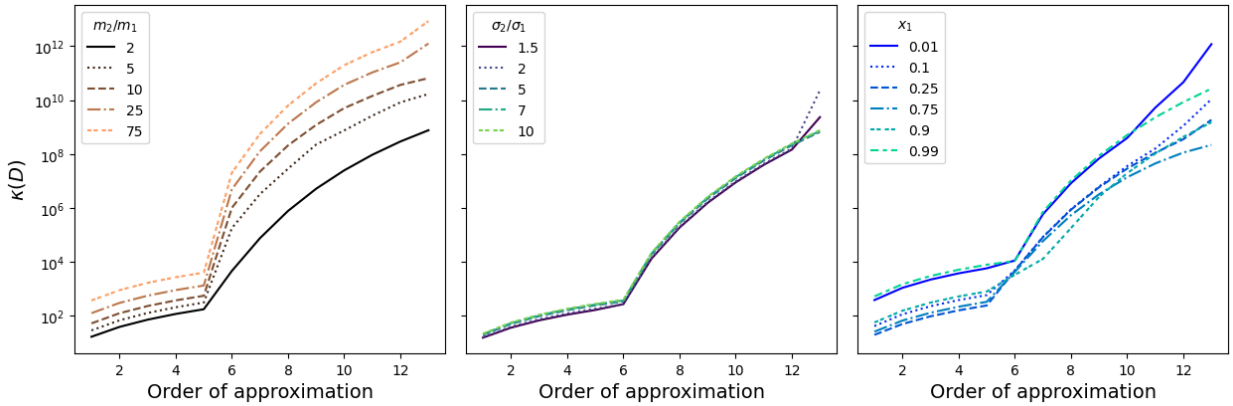

Figure 2.7: Condition number of the matrix $\underline{\boldsymbol{D}}_N$ of Equation (1.3) in various systems. Parameters for the computation are shown in Table 2.2.

the condition number $\kappa(\underline{\boldsymbol{D}}_N)$ was computed at varying mass ratios, HS-diameter ratios and compositions, as shown in Figure 2.7. Some of the trends in the instabilities can be understood from this analysis. Firstly, the condition number grows rapidly as the order of approximation goes past $N = 5$ for almost all cases shown. Secondly, increasing the mass ratio increases the condition number notably, but does not cause the "jump" at $N = 5$ to occur earlier. The HS-diameter ratio does not appear to have a significant effect on the condition number. Lastly, the trends seen in the condition number when varying the composition do not explain the stabilising effect of increasing the mole fraction of the lighter component, observed in Figure 2.6. Also noteworthy is the fact that at very high or low mole fractions, the "jump" in the condition number moves from $N = 5$ to $N = 6$.

In order to explain the trends observed when varying the composition, the alternative measure for error, ϵ_N^r presented in Section 1.1.1 was computed at various conditions, the results are presented in Figure 2.8. Firstly, note that the trends seen in the condition number are largely replicated when varying the mass ratios and the HS-diameter ratios. The condition number is a well established measure of potential error, so this agreement indicates that using ϵ_N^r as a measure for error is reasonable. The major difference in results between Figure 2.7, using the condition number and Figure 2.8, using ϵ_N^r is seen when the composition is varied. ϵ_N^r decreases with an increasing mole fraction of the lighter component. Recognise that while the condition number is a measure of potential error, ϵ_N^r is intended to be a measure of actual error. With this in mind, and observing that both $\kappa(\underline{\boldsymbol{D}}_N)$ and ϵ_N^r are small for small mass ratios, it appears that there is a stabilising effect of having a high mole fraction of low mass particles, that dominates the potential error introduced by very high or very low mole fractions of one component.

In summary, there are strong arguments to support that the observation of a divergent thermal diffusion ratio arising from the higher order Enskog approximations are the result of numerical error, rather than a physical phenomena. In this case the problem can likely be mitigated by appropriate scaling or preconditioning of the equations.

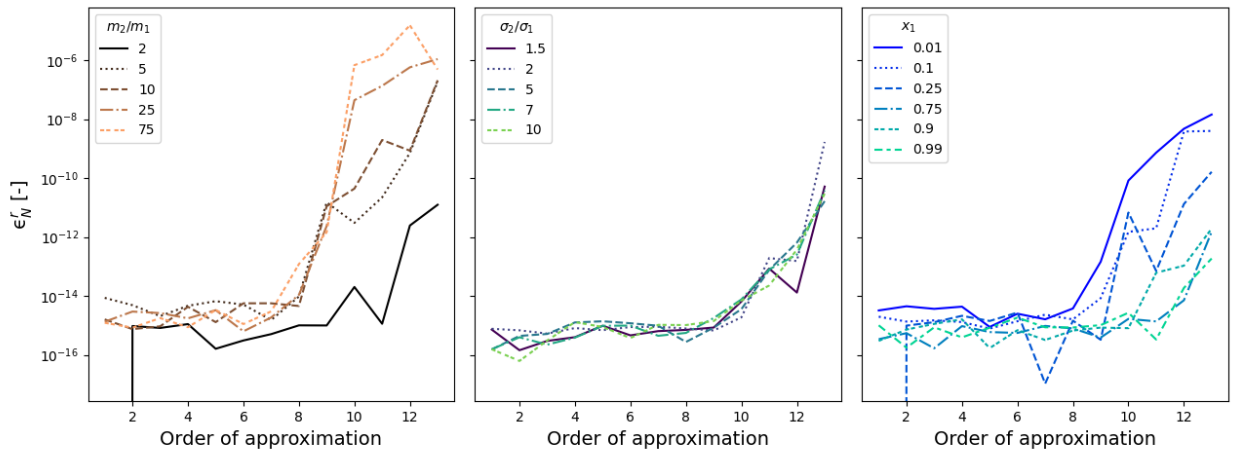

Figure 2.8: The relative error ϵ_N^r as a function of approximation order at various mass ratios, HS-diameter ratios and compositions. The value of parameters that were not varied are displayed in Table 2.2.

Table 2.2: Value of parameters that were held constant during systematic variation of the mass ratio, HS-diameter ratio and composition in Section 2.2. * Indicates the parameter that was varied. All computations were made at $T = 300\,\mathrm{K}$ and $\rho = 10\,\mathrm{mol\,m^{-3}}$.

Varied quantity	σ_1 [Å]	σ_2 [Å]	m_1 [$\mathrm{g\,mol^{-1}}$]	m_2 [$\mathrm{g\,mol^{-1}}$]	x_1 [-]
σ_2/σ_1	1	*	1	1	0.5
m_2/m_1	1	1	1	*	0.5
x_1	1	1	1	2	*

References

[1] S. Chapman and T. G. Cowling, *The mathematical theory of non-uniform gases*, 2nd ed. (Cambridge university press, Bentley House, 200 Euston Road, London, N.W. 1, 1964).

[2] H. Van Beijeren and M. Ernst, Physics Letters A **43**, 367 (1973).

[3] H. Van Beijeren and M. H. Ernst, Physica **68**, 437 (1973).

[4] R. C. Reid, J. M. Prausnitz, and B. E. Poling, *The properties of gases & liquids*, 4th ed. (McGraw-Hill Book Company, 1987).

[5] E. Tipton, R. Tompson, and S. Loyalka, European Journal of Mechanics - B/Fluids **28**, 353 (2009).

[6] R. Tompson, E. Tipton, and S. Loyalka, European Journal of Mechanics - B/Fluids **28**, 695 (2009).

[7] E. Tipton, R. Tompson, and S. Loyalka, European Journal of Mechanics-B/Fluids **28**, 335 (2009).

[8] S. Loyalka, E. Tipton, and R. Tompson, Physica A: Statistical Mechanics and its Applications **379**, 417 (2007).

[9] V. G. Jervell, "KineticGas," `https://github.com/vegardjervell/Kineticgas` (2021).

[10] E. N. Fuller, P. D. Schettler, and J. C. Giddings, Industrial & Engineering Chemistry **58**, 18 (1966).

[11] N. F. Carnahan and K. E. Starling, The Journal of chemical physics **51**, 635 (1969).